Airport Surveillance Processing Chain for High Resolution Radar

Gaspare Galati, Mauro Leonardi, Alessio Cavallin, Gabriele Pavan

***Abstract* — The paper focuses on the design of the digital processing chain of a Surface Movement Radar (SMR) for airport traffic in frame of A-SMGCS (Advanced-Surface Movements Guidance and Control System); in order to reach, or exceed, the demanding requirements for the A-SMGCS surveillance function, special attention has to be paid to SMR processing, whose main functional blocks are the CFAR (Constant False Alarm Rate) processor, the Plot Extractor and the Track-While-Scan (TWS). A description of these processing functions, tailored to a non-coherent, high resolution radar, and of their implementation is provided. The performance evaluation is accompanied by trials on recorded data, as obtained from a national research and development project called Fast Prototyping (FP) project (2001-2003) and its subsequent activities. The aim of this paper is to give a system view of the radar processing chain for high-resolution SMR, being rather different than standard surveillance radar.**

***Index Terms*—CFAR, Plot Extraction, Surface Movement Guidance and Control System, TWS.**

1. INTRODUCTION

THE increase of air traffic volume has led to the congestion of many airports. In particular the current surface traffic control systems are mainly based on the ability of tower controllers and

Gaspare Galati is with the Tor Vergata University, Rome, Italy (corresponding author - phone: +390672597417; fax: +3972597532; e-mail: gaspare.galati@gmail.com ; galati@disp.uniroma2.it . Address: Prof. Gaspare Galati, Tor Vergata University, DISP, Via del Politecnico 1, 00133 Rome, Italy).

Mauro Leonardi and Gabriele Pavan are with Tor Vergata University, Rome, Italy (e-mail: leonardi@disp.uniroma2.it , pavan@disp.uniroma2.it).

Alessio Cavallin, Ph.D. from Tor Vergata University, is now with Selex-Sistemi Integrati, Rome, Italy (e-mail: acavallin@selex-si.com).

operators to visually acquire and mentally maintain/update the traffic situation on the airport surface. Visual operations call for the reduction of the traffic (from many movements to a single movement at a time) in low visibility conditions as the standard level of safety must be guaranteed at any time.

An airport surveillance system must include both cooperating sensors and non-cooperating sensors; the main non cooperating sensor is the Surface Movements Radar (SMR), aimed to detect every object (aircraft, vehicle, obstacle…) of operational interest.

The Fast Prototyping (FP) project (Marco Polo airport, Venice 2001-2003) was an Advanced - Surface Movements Guidance and Control System (A-SMGCS) experimentation with a novel airport surveillance radar, which provided recorded data of an high resolution radar in millimetre wave band (*W* band). Raw radar data are usually quite difficult to collect in operational sites: this qualifying aspect encouraged us to test our work with real data beyond the common introductory analysis and simulation.

In airport applications, we have a very challenging scenario where different types of targets (aircraft, small vehicles, persons and even lost luggage) must be detected, while clutter echoes, coming from asphalt areas, grass areas and buildings, are present and even small objects (e.g. manholes, lights, signs, etc.) can result in a false alarm and can generate false tracks as well, as A-SMGCS both moving and fixed targets have to be located and identified, i.e. tracked. The clutter sources are variable both in space (depending on the airport layout) and in time (e.g. the grass height and its movements with the wind, the presence of weather phenomena such as rain, and so on). Therefore, a tight control of the false alarms is needed, and sophisticated Constant False Alarm Rate (CFAR) techniques become essential to keep false alarms under control and to guarantee a high probability of detection (usually P_{fa} is set below 10^{-6} and P_D at least 90% according to EUROCAE [1] and ICAO [2]).

Moreover, significant extraction problems also do arise because of the density of targets in the manoeuvring area and the fact that the target cross-range dimension depend on the distance from the radar.

Once plots are extracted, their positions must be tracked in real time by the Track While Scan (TWS) system. Surface targets show higher dynamics in their ground movements than in the en-route applications. Therefore, the tracker must be capable to follow a big number (up to

one thousand) of targets with high dynamics and changing in their orientation and speed within one second (the usual airport surveillance systems update time). On the other side, the allowed paths for the target are limited and well known so that this information can be useful to the tracking algorithms.

Summing up, the main challenges to radar surveillance in the A-SMGCS context are:

- Detection of both moving and standing targets in the presence of various type of clutter (grass, rain, point clutter);
- Presence of both extended targets such as commercial transport aircraft and point targets such as small vehicles, persons, objects (e.g. pieces of baggage);
- Need to track a big number of different type of targets (up to thousands) in a short time (0.5/1 second) in a very disturbed (false targets) condition
- Need to guarantee the continuity of the tracks even in clutter area (e.g. when a target, by error, enters a grass area);
- Need to resolve close-by targets even of different type (e.g. an aircraft and a service vehicle).

A typical simplified scheme of the radar processing in shown in Fig. 1.

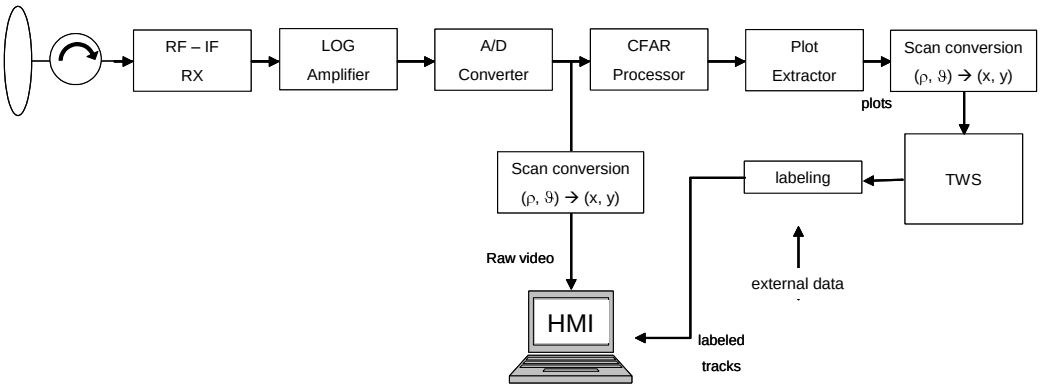

Fig. 1. Receiving chain of a typical surface movements radar (SMR).

After the analog chain (with a non-coherent receiver and a log-amplifier) and the A/D conversion, the digital chain consists of the CFAR threshold system, the Plot Extractor and the TWS.

The main aim of the paper is to evaluate the performance of algorithms and novel solutions

using high resolution surface radar to cope with the A-SMGCS challenges, not only to propose new techniques and algorithms but, mainly, to define the right processing scheme (from the sensor to operational display) to exploit the high resolution of the sensor with a cheap Commercial Of The Shelf (COTS) architecture.

This paper is organized as follows. In Chapter 2 the airport environment and the raw radar data used for trials on a real scenario are presented. In Chapter 3 the analyses of the CFAR thresholding technique are described highlighting the problems related to airport applications. Chapter 4 focuses on the plot extraction algorithms and on estimation of the bearing angle, i.e. a further measurement available only in the case of high resolution radar. Finally, in Chapter 5 different tracking solutions and some related performance results are shown.

2. THE OPERATIONAL SCENARIO

In the Fast Prototyping project the sensor was a *W*-band radar. The radar was installed in the Apron area of the Venice – Marco Polo airport on a trellis at 22-m above the ground. The main characteristics (nominal values) of this pulse radar are:

- operational frequency : 95 GHz;
- peak power : 1 kW;
- pulse repetition frequency (PRF) : variable, up to 32 kHz;
- pulse length : 20 ns (i.e. range resolution of 3 m);
- azimuth beamwidth : 0.18° (cross-range resolution 3 m @ 1 km);
- range coverage: up to 3 Km in clear weather, 2 Km in fog with 50 m visibility, better than 1.2 Km in rain (at the rainfall rate of 16 mm/h, as from EUROCAE/ICAO specs and recommendations [1], [2]).

During the radar scan, the echo is acquired along M azimuth sweeps (each sweep having N range bins); the digitised echo (8 bit represent the amplitude in logarithmic scale for each resolution cell) is therefore stored in a file representing the $N \times M$ radar cells in ρ, θ coordinates (typical values for N and M being 1024 and 4096 respectively). This "image" of the radar reflectivity is fed to the processing blocks which create the plots and the tracks to be presented on the HMI (Human Machine Interface). All the processing chain is performed by two

standards PC:

- one equipped with an acquisition/digitalization card and a processing card (FPGA and DSP) which sample the signals coming from the sensor, and performs the detection (CFAR) and the plot extraction,
- one used to track the targets,

while other PC's can be used as HMI.

3. CONSTANT FALSE ALARM RATE THRESHOLD

An operational airport scenario contains different types of clutter. For example Fig. 2 shows the raw radar images in ρ, θ coordinates; in particular, the histograms for the different areas (concrete, grass, etc.) are shown. In this situation, asphalt radar echo is slightly above to noise level, while grass has a stronger echo depending on the wet/dry status of vegetation, on the wind speed and on the length of stems. Two types of grass are considered depending on their radar echo, stronger and weaker respectively.

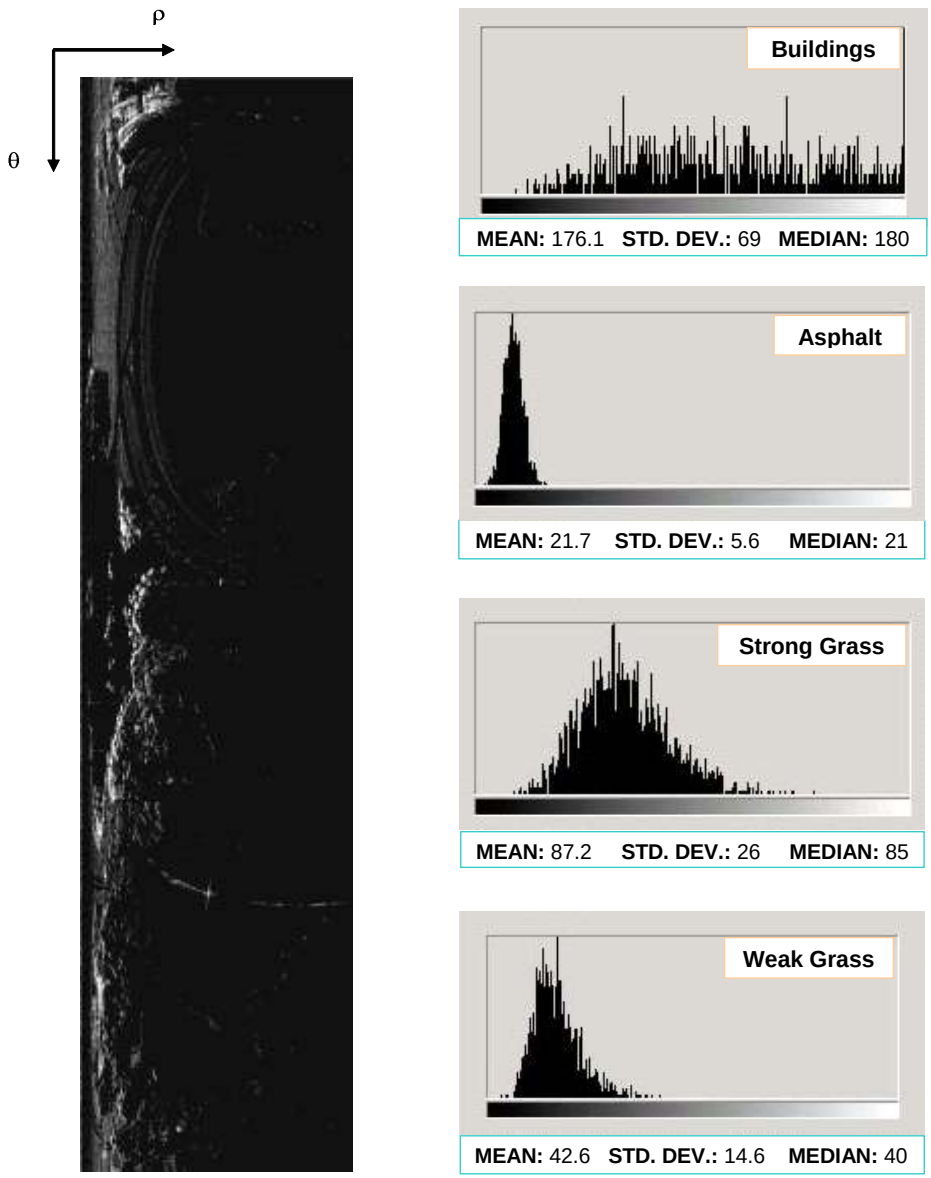

Fig. 2. Radar image (before scan conversion) of Venice airport (13 Nov. 2002) in clear weather. Pixel amplitude values after the LOG amplifier are integers between 0 and 255. Histograms of asphalt (taxiways, runways, Apron), grass and buildings are shown on the right side. The abscissa values are from 0 to 255.

The estimates of amplitude statistics (mean value and standard deviation) of clutter are used to set the CFAR parameters, as discussed below.

The aims of the proposed CFAR are (apart from maintains the False Alarm constant):

- To be simple to be implemented in a FPGA/DSP board;
- Capable to take care of different type of clutter;

- Capable to detect also fixed targets;
- Capable to detect also in rain clutter conditions;
- Fast, as all the processing from the sensor to the HMI must be executed in a few hundreds of millisecond.

Is also important to note that the proposed CFAR (and also the remaining of the system) must work on all the coverage cells (not only in the manoeuvring area but also in the grass etc.) without any censoring process, differently of most of SMR systems already used. This is requested to detect and manage also situation related to security or emergency. This assumption makes more stringent the requirements in terms of computational load and speed.

Constant False Alarm Rate techniques can be divided into two main groups: (1) CFAR based on spatial statistics and (2) CFAR based on temporal statistics.

For the problem at hand, we examined different solutions, such as the Cell Averaging threshold (spatial) and the classical Clutter Map (temporal).

A. Cell averaging vs. Clutter Map CFAR

A spatial CFAR computes the threshold on the basis of the echo amplitude received at the same scan from resolution cells next to that under test. The simplest spatial CFAR technique is the Cell Averaging CFAR (CA-CFAR) [3], based upon the mean value of the echoes amplitude. This technique is suited to spatially homogeneous environments [4] where echoes from different range resolution cells have the same probability density function. However, in an airport scenario clutter is spatially non-homogeneous due to transitions to asphalt or to grass, variations in the vegetation type and density and so on. Such clutter edges may increase the probability of false alarm, P_{fa}, or may even mask a target. Moreover, multiple targets in the same window increase the CFAR threshold, masking or even splitting the primary target. Therefore the well known CA-CFAR [5] may be ineffective or scarcely effective. Alternative schemes ([6]-[9]) have been developed to address this issue at the price of a greater computational load. A possible solution for non-homogeneous environment applications is described in papers [10] and [11].

A clutter map CFAR (CM-CFAR) [13] sets the threshold on the basis of a weighted average of the echo amplitude in the previous scans for each resolution cell. A bi-parametric CM-CFAR (i.e. one setting the threshold by estimating two parameters of the density function of the clutter amplitude), which theoretically has a better behaviour [3], [4], fails for clutter rapidly varying in time, since it also estimates the standard deviation of the clutter. Therefore, in airport applications, where both targets and moving rain cells can produce quick variations of the estimates, a mono-parametric CFAR is to be preferred [12]. The main drawback of temporal CFAR is the self-masking of slow or fixed targets [4]. When a target remains in its position for a long time (w.r.t. the updating rate) the threshold increases due to the target itself. The risk is that the target is no longer detected. This happens, for example, when targets await at the stop bar. Therefore, CM-CFAR can be improved introducing anti-masking methods. Among them, the one proposed in [12], i.e. amplitude limitation at the CFAR input (to avoid a too quick raise of the threshold) followed by "freezing" of the threshold (to avoid a too large increase of it) resulted mostly effective.

As already stated, a main problem in radar detection of airport surface targets is the presence of rain. Rain phenomena, e.g. those related to convective cells, have a space-time variability which can degrade CFAR performance. The rain echo (in the most used bands, i.e. X and K, and, even more, in W band) can be very strong, causing missed detections due to a quick increase of the threshold, or false alarms. This phenomenon must be carefully considered as airport systems must operate in strong rain (up to 16 mm/h rainfall rate) [2].

B. CFAR processing for a specific application: the airport environment

In airport applications some improvements on CFAR techniques can be performed. Spatial CA-CFAR can be modified using fixed macro-cells (some hundreds of resolution cells) containing clutter of the same type (asphalt or grass). A promising improvement is to merge spatial CFAR and temporal CFAR, leading to Hybrid CFAR processors [13], [14][15].

In our Hybrid CFAR processing, firstly proposed in [16], the spatial average of resolution cells in the same macro-cell is used to perform the time-domain average; more advanced processing such as Order Statistics or Censored Mean [3] are not considered because of the

aforementioned problems with extended targets and of their high computation burden not always compatible with the hardware used. The macro-cells, whose typical dimensions are much greater than the radar resolution cell, are designed according to the airport (reflectivity) map in order to contain mostly homogeneous clutter. Fig. 3 shows the block diagram of the proposed Hybrid CFAR.

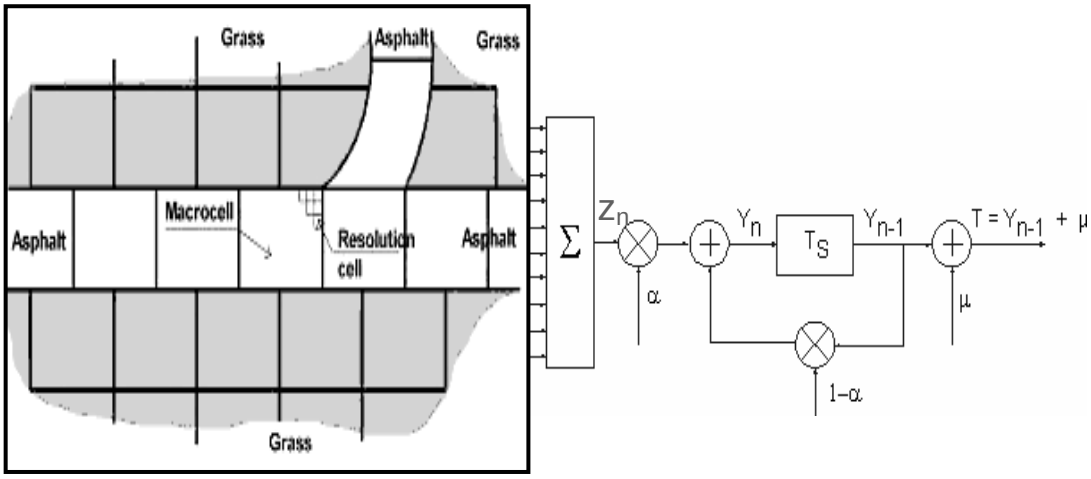

Fig. 3. Hybrid CFAR architecture: n is the scan number, T_s the scan period, α the feedback coefficient of the loop filter, μ a threshold coefficient, and T the CFAR threshold.

The CFAR threshold [16] is computed on the basis of an average of "macro- cell" amplitudes (see Fig. 3):

$$Z_k(n) = \frac{\sum_{i,j} x_{i,j}(n)}{N_{cell}(k)} \qquad (1.1)$$

where $x_{i,j}(n)$ is the echo amplitude value at time (scan number) n in the radar resolution cell i, j , $Z_k(n)$ is the average of the echo in the macro-cell k at time n and $N_{cell}(k)$ is the number of radar cells in the k-th macro-cell. We set the macro-cell dimensions to the order on one hundred meters (both in range and azimuth), so that masking phenomena and the variations of clutter power within each macro-cell are of very limited extent.

We chose the constant μ in Fig. 3 as to guarantee the expected P_{fa} (typically 10^{-6}) and the feedback coefficient α of the recursive filter to have an equivalent memory of 64 scans (i.e. a time constant of the order of a minute), which, according to simulations and experiments, gives

a fairly good time response to clutter variations.

C. Simulations and Trials

We tested the CFAR techniques as described in the previous paragraphs; remember that still (or very slow) targets require anti-masking techniques and some limited increase of P_{fa} after their detection must be accepted to mitigate the masking phenomenon which could be more dangerous [12].

For the proposed Hybrid CFAR (unlike the Clutter Map one), the target echo is "diluted" in the macro-cell. Therefore, updating of the detection threshold (Fig 3) is less influenced by the other echoes in the same scan. We found that the probability of detection on asphalt clutter keeps near 90% for SNRs greater than 19.5 dB even in the critical simulation of a small target (for example a "Follow Me" car) which occupies one radar resolution cell in the macro-cell where also an extended target (aircraft) is present .

Obviously, for the Hybrid CFAR the masking depends on the macro-cell dimensions, on the SNR and on the number of targets. In fact, a target can be masked both by itself (self-masking) and also by the presence of other targets which are in the same macro-cell. We investigated and simulated the behaviour of the proposed CFAR processor when a point target (e.g. a person or a small vehicle, smaller than the radar resolution) and extended targets enter the macro-cell simultaneously; some examples are shown in Table I. In all cases the reduction of the probability of detection for the point target, due to the presence of other targets, is acceptable for the A-SMGCS operation.

TABLE I

HYBRID CFAR: PROBABILITY OF DETECTION FOR A POINT TARGET (P1) WITH EXTENDED TARGETS (E2, E3) IN THE SAME MACRO-CELL

No. of targets	**No. of cells**	**SNR (dB)**	***P_D (%)* for P1**	
			1 st scan	**15 th scan**
2 Targets	P1 = 1 cell E2 = 66 cells	$SNR_{P1} = SNR_{E2} = 20.5$	94	92
		$SNR_{P1} = SNR_{E2} = 19.5$	91	87
2 Targets	P1 = 1 cell E2 = 66 cells	$SNR_{P1} = 20$ $SNR_{E2} = 50$	92	86
3 Targets	P1 = 1 cell E2 = 66 cells E3 = 66 cells	$SNR_{P1} = SNR_{E2} = SNR_{E3} = 20.5$	94	89
		$SNR_{P1} = SNR_{E2} = SNR_{E3} = 19.5$	90	84

We also conducted trials on real data recorded at Marco Polo airport. In particular Fig. 4 presents an example of the CFAR techniques applied to the recorded data as shown in Fig. 2.

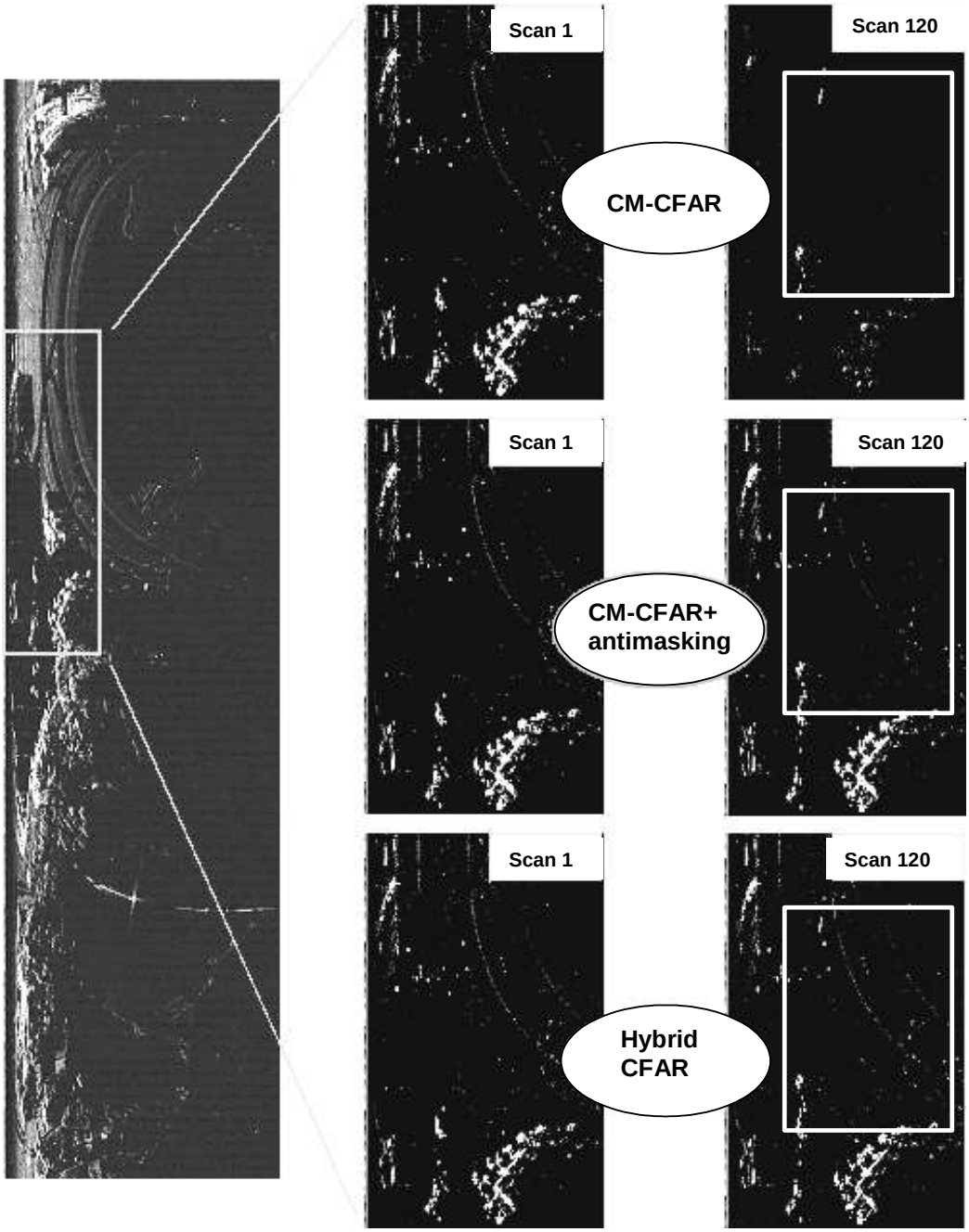

Fig. 4. Output images from CFAR processing (scenario of Fig. 2) at the 1st and 120th scan (revolution speed at 60 rpm): Clutter-Map CFAR (top), Clutter-Map CFAR with Antimasking (center) and Hybrid CFAR (bottom).

The results show that the bottom image (Hybrid CFAR @ 120^{th} scan) is the best, since more details in the movement area (white box in the figure) are still visible. CM-CFAR shows a strong masking effect after 120 scans, which reduces heavily the probability of detecting targets both on asphalt and on grass. Better performances are achieved using the anti-masking

technique [1], [15] based on the limitation of the input amplitude and the freezing of the threshold after the detection (labelled CM-CFAR + anti-masking in Fig. 4), even if it cannot fully solve the self-masking problem for slowly moving or steady targets.

In conclusion Hybrid CFAR solution is promising since it is less sensitive to the self-masking with respect to the CM-CFAR, has an acceptable masking by other targets as the loop filter smoothes the time variation of the signal, and guarantees low detection losses. Its performance in case of rain depends on the macro-cells dimensions. Reduced radial dimension for the macro-cells - therefore increasing the number of cross-range cells - provides a better behaviour in rainy weather. In conclusion Hybrid CFAR, if well designed, produces the benefit of the Clutter map in the case of multitargets without the problem of automasking and has the benefit of CA-CFAR in the case of standing targets.

4. Plot Extraction

The extractor downstream the CFAR threshold correlates radar resolution cells, where detection occurred, by criteria based on the spatial adjacency, to make a plot. Such logic requires a trade-off between the conflicting requirements to distinguish nearby targets (including extended targets such as an aircraft and point targets due to small objects – occupying only one or a very few resolution cells - such as luggage or trolleys) and the risk to split an extended target (up to hundred cells if very close to the radar) into two or more plots. Also in this case the extractor must be simple due to the fact that must be hosted in a COTS hardware.

A. Plot Extraction method

The association logic considers each radar sweep (along the current azimuth θ) and inside the sweep each cell (i.e. each range bin). The correlation region is represented by the following expression, which considers a distance of *M* pixels [17]:

$$i_x , j_x \quad : \left| i_k - i_x \right| + \left| j_k - j_x \right| \leq M \tag{1.2}$$

where $i_{k,x}$ and $j_{k,x}$ represent the indexes (i.e. range and azimuth) of the considered pixels and with *k* being the index of the cell under test.

The extraction process is performed inρ, ϑ coordinates. This implies that an extended target has a cross-range extension that linearly increases with the distance from the radar. In fact, for a target the ratio between the number of azimuth cells when close to the radar and those far from the radar can be up to an order of magnitude. To guarantee correct association, the logic in (1.2) must be parameterized within circular rings centred on the radar. The extraction parameters in each ring will appropriately vary depending on the distance from the radar itself.

Once the correlated pixels are identified, the extraction tool computes the characteristics of each plot (i.e. target): geometric centre of gravity, extent in two directions (range and azimuth), number of cells, mean and maximum intensity. This implementation of the Extractor (simple and well known) was chosen to generate the input to an additional novel processing that uses the shape of the plot to extract additional information from the target, in particular the bearing angle.

B. Bearing Angle Extraction

The high-resolution capabilities of the *W* band radar have been demonstrated in [18]; this fact has encouraged research activities to extract the bearing (or "orientation") angle of the aircraft target, to be used:

- for runway incursion monitoring
- as visual aid of the controller in the HMI
- in the tracking of mobiles, in particular aircraft, to improve the tracking performance.

As explained before, the extraction of the target information of the plot is performed inρ, ϑ coordinates. Instead, the orientation angle has to be obtained in *x*, *y* coordinates. Hence, the radar image is converted from polar to rectangular coordinates (digital scan conversion) and then sent to bearing angle extractor. We investigated three methods to extract the bearing angle and proposed a fourth one:

(1) the Hough transform: in the Hough space the accumulation points identify the bearing angle of the main axes of the object. The axes of symmetry, such as the airplane fuselage or the wings, are identified by the local maxima in the Hough transformed space [19].

(2) the Moments of Inertia: is based on the estimation of the primary axis of inertia of the aircraft image. The main axis is evaluated in a reference system whose origin is the target centre

of gravity so that it represents the axis whose moment of inertia is the lowest [20].

(3) Correlation with Templates: in this technique it is supposed to have a data base with templates (radar images) of the most common commercial aircraft for different bearing angles, e.g. from 0° to 360° at steps of 1.2° and at typical distances from the radar (e.g. 100, 300, 500 and 1000 m). By performing the 2-D correlation between the real radar image and the template it can be possible to determine both the bearing angle of the aircraft and its type [20].

(4) The Proposed approach (denoted by H/C). The correlation method is very costly in terms of computation; then we applied this method downstream of the Hough transform (Hough → Correlation, for short: H/C). The aim is to exploit the correlation capabilities only with a reduced set of angles and displacements. The greatest values of the Hough transform identify the *m* most probable directions (i.e. the orientation angles) to be inserted in the 2-D correlation. The maximum correlation value amidst the Hough transform candidates represents the H/C estimate. In this way even if the Hough estimates fails of about 10°, the accuracy of the Correlation can compensate the error of the first guess. Moreover, the number of correlations to be performed is limited to 10-20.

We found that the proposed approach (H/C) provides an error for the bearing of about 3° rms. The other methods present worse performance: the Hough method r.m.s. error is up to 6.5° while the r.m.s. error of the Moments of Inertia is 12.5° at best. A more detailed description of these results on simulated data is presented in [21].

An example of bearing angle extraction is reported in Fig. 5: the target is a B737 – 400 aircraft on the runway of Marco Polo Airport in Venice (raw video in Fig. 6). The evaluated direction of the fuselage is superimposed to the image. This trial is only qualitative as the actual angle is unknown (unfortunately the recordings are not supported by other independent measurements so the true bearing angle is not available), but one can assume that the pilot usually follows quite well the position and the direction of the centre line of the runway.

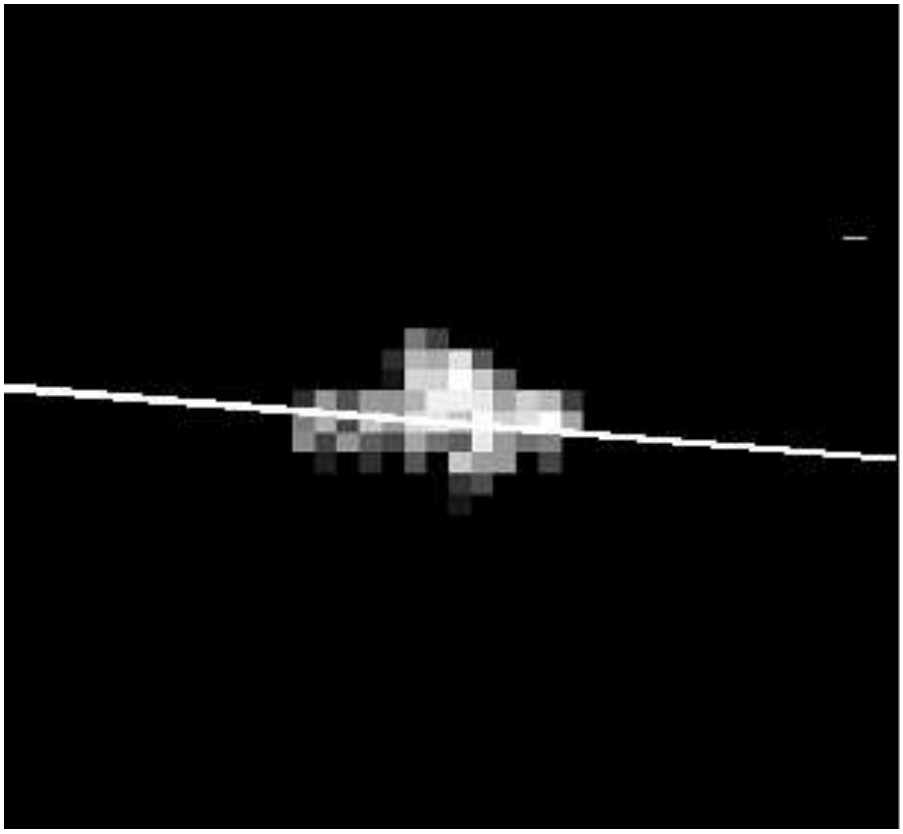

Fig. 5. Example of the bearing angle extraction using the Hybrid Method (after CFAR processing) applied to the target in Fig. 6

Fig. 6. Image of a B737-400 (overall length=36.4 m, wing span=28.9 m). Marco Polo airport, Venice. (Digital Scan Conversion applied). 3 April 2003

5. TRACKING FILTER IN TWS

In a multi-target environment, as in the case of an airport scenario, an important feature is the capability of simultaneously managing a great number of tracks with a high level of accuracy [21], [22]. The goal of the proposed algorithms is to improve the tracking accuracy, and more generally, the state estimation for the target.

This aim must be reached using a single commercial PC, that manages up to thousands of target per second. In this case Multi Target Tracking in clutter scenario is performed with the Multi Hypothesis Tracker (MHT) [23]-[25] that use most of the computational power to manage the tracks and all the Hypothesis. The tracking (track estimation process) filter must be simple due to the risk to overload the system.

In most airport applications, simple α-β filter or Kalman filters are used ([23]-[27]), making a trade-off between performance and computational load (that must be as low as possible due to the necessity to manage a large number of targets in a fraction of one second).

This kind of filtering, however, requires a difficult choice between:

- Broadband Filter: low accuracy due to the measurement errors and large plot-to-track association window, which involves a high probability of false alarm and wrong association.
- Narrowband filter: more accurate position estimates in rectilinear motion but high probability of losing tracks when a change in the motion model or parameters of the target occurs.

The dynamics of a target in an airport (constant velocity motion on the Taxiways, high turning rate motion on the Taxiway-Runway connections and in the Apron, accelerated motion in the Runways), calls for an hybrid solution that can manage all the changes of motion of the target. This issue can be faced with Interacting Multiple Models (IMM) filtering [24] but at the cost of a high computational load that not always is acceptable. We evaluated some alternative of simpler filters that use the principle of the reactive adaptation to reduce the computational load: Adaptive α-β filter and Adaptive Kalman Filter ([24]-[27]). Moreover since the areas and trajectories of the allowed movements on the airport surface are well known and various maps are already used in airport management, we use these maps to improve the tracking performance of the A-SMGCS, leading to other three types of filtering: Topographic α-β

Filter, Topographic Kalman Filter, Topographic IMM [22]. Finally we consider also the use of the bearing angle information coming from the extractor.

A. Standard, Adaptive and Topographic Tracking

Adaptive filters change the values of their parameters when a manoeuvre is detected; in particular the prediction residual (i.e. the difference between predicted and measured positions) is monitored to detect a change of the motion model [24]-[27].

Let us assume a target with constant velocity motion In the proposed adaptive α-β filter the parameters α_k and β_k are selected at each scan k among the values stored in a table (with size N):

$$\begin{aligned} \alpha_k &= \alpha(n) \\ \beta_k &= \beta(n) \end{aligned} \tag{1.3}$$

with the parameter $n = 1,...,\mathrm{N}$ variable according to the following logic:

$$\begin{aligned} & n = n+1 \quad \text{if} \quad \textit{innovation} < R_t \ \text{and} \ n < N_{\max} \\ & n = n-1 \quad \text{if} \quad \textit{innovation} > R_t \ \text{and} \ n > N_{\min} \\ & n \ \text{remains unchanged, otherwise} \end{aligned} \tag{1.4}$$

The $\alpha(n)$ and $\beta(n)$ values are such that the filter bandwidth (i.e. the response speed) is narrower (slower) for n increasing, as shown in Table II. The threshold R_t is defined as the 60% (empirically selected) of the gating window's size; $N_{\max}, N_{\min}$ are the size of the table. The innovation is given by $\underline{y}_k - \underline{x}_{k,k-1}$, where $\underline{y}_k$ are the measurements and $\underline{x}_{k,k-1}$ the position state of the target [23].

In the Adaptive Topographic α-β filter, the α_k and β_k values are restricted, zone by zone, according to topographic information (Figure 8). This means that the map forces the filter to work in a part of the table that is appropriate for the zone where the target actually is (the filter uses high values for α and β in the manoeuvring areas, like in the Taxiway-Runway connections). Topography information grants better accuracy, as the filter can "predict" the target change of motion and speed up to the transient in this change.

In particular the parameter n varies as follows:

$$(1.5)\qquad \begin{aligned} n &= n+1 \quad \text{if} \quad innovation < R_t \ \text{and} \ n < N_{\max}(\underline{y}_k) \\ n &= n-1 \quad \text{if} \quad innovation > R_t \ \text{and} \ n > N_{\min}(\underline{y}_k) \end{aligned}$$

where N_{max} and N_{min} are dependent on a suitable map, see Table II.

TABLE II

α-β VALUES STORED IN THE TABLE AND SELECTED TIME BY TIME

n	Alpha	Beta
1	1	1
2	0.833	0.7
3	0.7	0.409
4	0.6	0.27
5	0.5	0.2
6	0.4	0.1
7	0.3	0.05
8	0.2	0.025
9	0.1	0.015

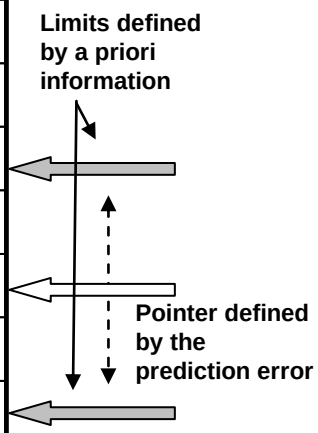

In the Adaptive Kalman filter, the driving noise $\sigma_{v,k}$ is changed scan by scan with the same operating principle that is used in the Adaptive α-β filter for α_k and β_k, i.e. according to the innovation magnitude [23], [24]:

$$(1.6)\qquad \sigma_{v,k} = \sigma_v(j)$$

where $j = J_{\min},..., J_{\max}$ is a pointer to the table that stores the values of σ_v. If the innovation is smaller than the threshold R_t (60% of the gating window's size) the plant noise decreases, otherwise the plant noise increases.

In the Topographic Kalman the equations become:

$$(1.7)\qquad \begin{aligned} j &= j+1 \quad \text{if} \quad innovation < R_t \ \text{and} \ j < J_{\max}(\underline{y}_k) \\ j &= j-1 \quad \text{if} \quad innovation > R_t \ \text{and} \ j > J_{\min}(\underline{y}_k) \\ j &\ \text{remains unchanged, otherwise} \end{aligned}$$

as in the α-β case.

To evaluate the proposed method the IMM techniques were also investigated [22]; we considered a classical IMM solution with five Kalman filters, i.e. one for rectilinear motion, two for right hand curvilinear motion and two for left hand curvilinear motion as proposed in [23][24][28][29].

In this case the parameters to be optimized are:

- the dynamic model for each filter (that are different rate of turn for a right and left circular motion , or a simple rectilinear motion;
- the *a priori* probability for each filter, from which the mixing probabilities matrix is computed;
- the power of plant noise for each filter.

The Topographic Information was also included using different a priori probability matrix of the model depending on the position of the target (Figure 8 show the most probable filter for each zone of a particular trajectory for a landing airplane).in this way we force the filter to use some filters instead of others in the state estimation process.

Trials were performed both with simulated data and with real data also to correctly tune the proposed filter. A summary of the results for the various tracking algorithms is reported in Table III and in Fig. 7 (Fig. 8 shows the simulated trajectory for the mobile).

TABLE III

AVERAGE PERFORMANCE OF THE THREE TOPOGRAPHIC FILTERS IN TERMS OF TRACK ERROR REDUCTION WITH RESPECT TO THE MEASUREMENT ERROR AND IN TERMS OF COMPUTATIONAL LOAD

	Error reduction (%)		**Computational Load (flops)**
	Standard	**Topographic**	
α-β	21	37.68	35
Kalman	23.4	44.81	700
IMM	46.31	50.8	6500

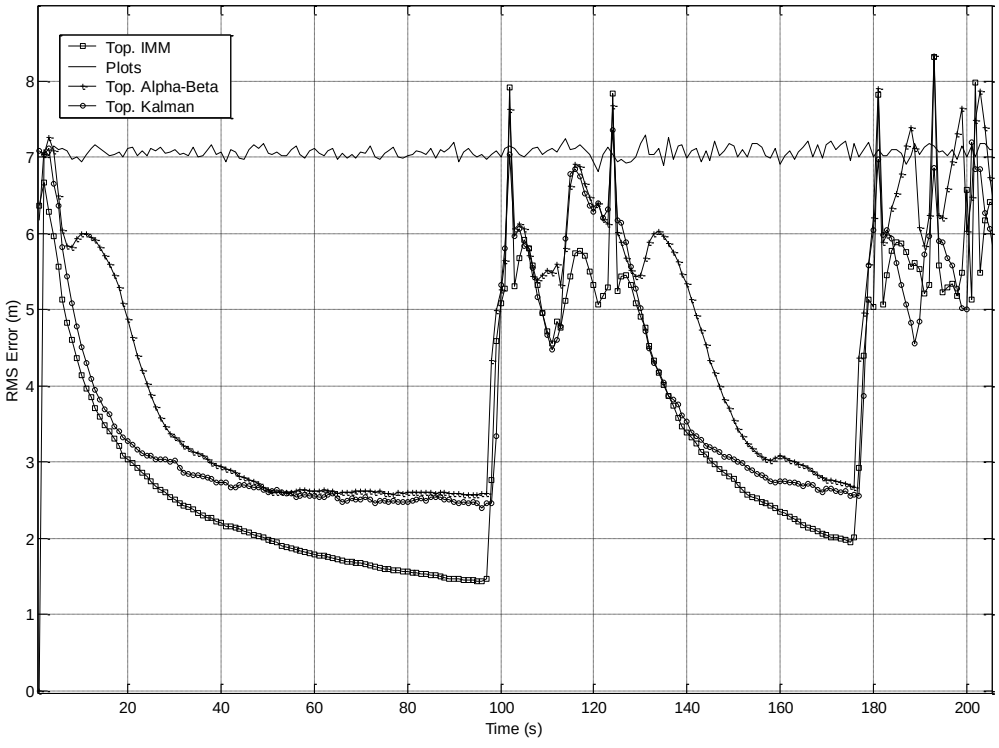

Fig. 7. Comparison of the performance in terms of RMS error of the three Topographic algorithms proposed for each scan of the sensor (207 consecutive scans, one scan per second). Simulated Data with 2000 trials.

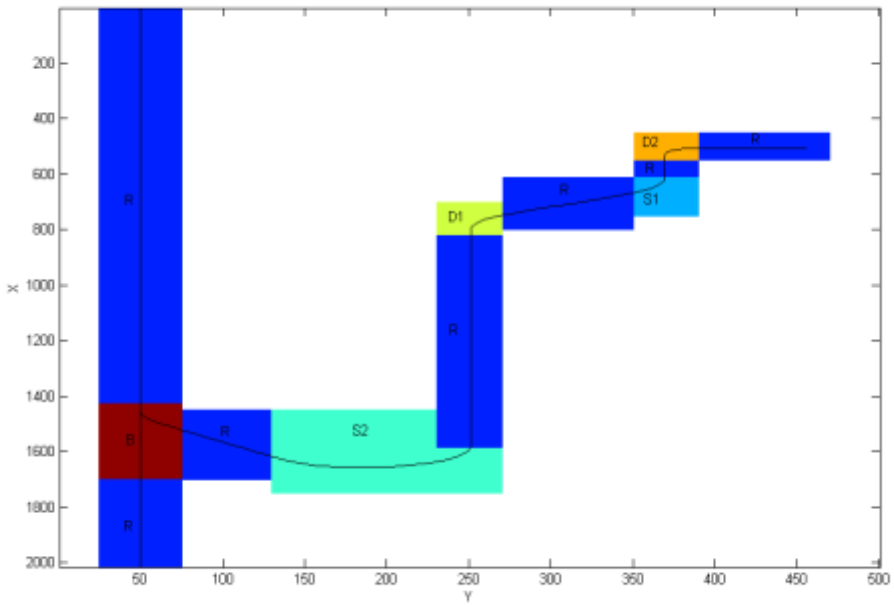

Fig. 8. Path used to test the various tracking algorithms, in rectangular coordinate system, x (m) and y (m).

The best results are performed with IMM filtering but with big amount of needed computational power.

A good trade-off for an A-SMGCS can be the Topographic Kalman Filter [30] [31] that has the following advantages with respect to the other algorithms:

- very high performance in terms of accuracy error and very good performance in terms of Gating Probability and Wrong Track Termination;
- low computational load as compared to the IMM solution;
- capability to change the gating window's size dynamically and capability to supply the prediction precision's estimation (and so to define the gating windows size).

B. Tracking with the Bearing Angle Measurement

As described before, thanks to the high-resolution of the *W*-band radar, the estimated bearing (or "orientation") angle of the target could be used to upgrade the dynamical model of the target. This method can be integrated within different trackers.

Using an Extended Kalman filtering a three dimensional measurement space results : two coordinates (i.e., x, y) and the bearing angle (i.e., ψ) of the target. Then the third component

of the innovation vector is the difference between the measured angle and the predicted angle (the predicted angle is computed using the predicted velocity component, $\psi_k = arctg(\nu_y / \nu_x)$). The third component can be used to detect the bearing changes (Bearing Angle Sensor), therefore detecting if the target is changing its motion model [24], [25].

We considered an additive zero mean value Gaussian noise with standard deviation $\sigma_\psi(rad)$ and assumed the rms error of the bearing angle estimation as that of the H/C method described in 4.B, i.e. $\sigma_\psi = 0.0523$. Denoting by ν_{ψ_k} the innovation component related to the bearing angle, its distribution becomes:

(1.8) $$\nu_{\psi_k} = N_\psi(0, \sigma_\psi)$$

and two different values for the threshold *c* were computed fixing the probability of false manoeuvre detection (*c=0.13* for $P_{fa}=10^{-2}$ and *c=0.17* for $P_{fa}=10^{-3}$).

When the absolute value of the third component of the innovation is smaller than *c* it can be decided that the mobile is in rectilinear motion with a small plant noise:

(1.9) $$\sigma_\nu = 0.1 m/s^2$$

When the absolute value of the third component of the innovation is larger than *c* the mobile is assumed to be turning and the value of σ_ν, to better follow the measurement instead of the model (that, in this case, is not perfectly matched to the real environment), is empirically defined and set to:

(1.10) $$\sigma_\nu = (10 + |\underline{\hat{v}}| \cdot |\underline{\nu_{\psi_k}}|)^{1/2} \ m/s^2$$

where $|\underline{\hat{v}}|$ is the estimated velocity of the target.

Simulation results for 2000 trials in the same hypothesis of 5.A are shown in Fig. 9. The peak error in the manoeuvring part of the trajectory is drastically reduced. These results are slightly better than those coming from the topographic approach.

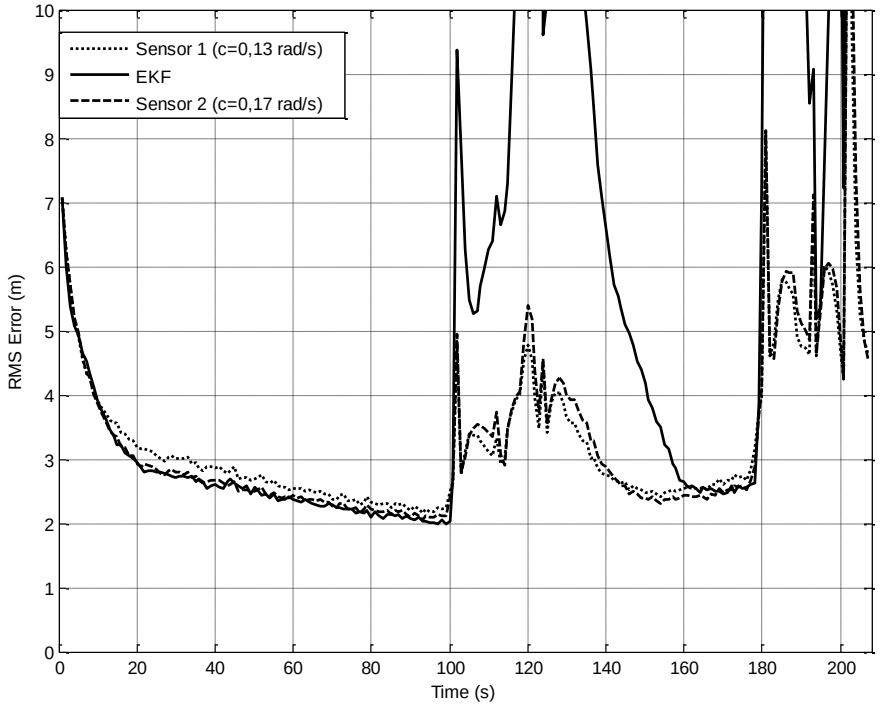

Fig. 9. Performance of tracking with and without bearing angle extraction (207 consecutive scans, one scan per second). Simulated Data with 2000 trials.

6. CONCLUSION

In the paper the main components of the processing chain of a high resolution radar for airport surveillance (i.e. a SMR) were investigated and some solutions were proposed using both simulation and real data.

The problems coming from a very complex scenario (large and small targets, high dynamic target motion, different types of clutter) call for an overall view of the digital processing with combined design of the blocks of the receiver chain: CFAR Thresholding, Plot Extraction and Track While Scan.

In the particular case of Fast Prototyping Radar, installed at the Venice Airport, we suggested a two-step solution: the first step is the use of Hybrid CFAR and Topographic Kalman Filtering; the second step is the introduction of bearing angle extraction and of the manoeuvre sensor in the TWS, provided that the computational load will become acceptable for real time operation.

In addition to trials with simulated and real data, human factor studies were performed in the Venice airport and other Italian and foreign airports to interview the controllers, to analyze the installed systems and to collect raw data.

ACKNOWLEDGMENT

We would like to thank ENAV Spa and the companies Thales ATM and Oerlikon Contraves (now Rheinmetall, Italy) for their valuable cooperation.

REFERENCES

[1] ED-87A MASPS for Advanced Surface Movement Guidance and Control Systems, Eurocae 1997.

[2] Doc 9476-AN/927 Manual of Surface Movement Guidance and Control Systems (SMGCS), ICAO 1986.

[3] Rohling H., "Radar CFAR thresholding in clutter and multiple target situations", *IEEE Transactions on Aerospace and Electronic Systems*, vol. 19, no. 4, 1983.

[4] Gandhi P. P., Kassam S. A., "Analysis of CFAR processors in nonhomogeneous background", *IEEE Transactions on Aerospace and Electronic Systems*, vol. 19, no. 4, 1988.

[5] Rohling H., "25 Years Research in range CFAR", *Proceedings of IRS 2003*, Dresden, 2003.

[6] Ozgunes I., Gandhi P. P., Kassam S. A., "A variably trimmed mean CFAR radar detector", *IEEE Transactions on Aerospace and Electronic Systems*, vol.28, no.4, 1992.

[7] Meng X., He Y., Lu D., Peng Y., "Performance analysis of a new Greatest of Selection CFAR detector", *CIE International Conference on Radar*, Beijing, 8-10 October 1996.

[8] He Y., "Performance of some generalised modified order statistics CFAR detectors with automatic censoring technique in multiple target situations", *IEE Proceedings on Radar, Sonar and Navigation*, vol.141, no.4, 1994.

[9] Lim C.H., Lee H.S., "Performance of order-statistics CFAR detector with non coherent integration in homogeneous situations", *IEE Proceedings Radar and Signal Processing*, vol.140, no.5, 1993.

[10] Lops M., "Hybrid Clutter Map L-CFAR Procedure for Clutter Rejection in Non homogeneous Environment", *IEE Proceedings on Radar, Sonar and Navigation*, vol.143, no.4, 1996.

[11] Lops M., Willett P., "Ll-CFAR: a Flexible and Robust Alternative", *IEEE Transactions on Aerospace and Electronic Systems*, vol.30, no.1, 1994.

[12] Galati G., Leonardi M., Magarò P., Cavallin A., "Multidimensional CFAR techniques in High Resolution Radar for Airport Surveillance Applications", *Proceedings of IRS 2003*, Dresden, 30 Sept. - 2 Oct. 2003.

[13] Khoury E.N., Hoyle J.S., "Clutter Maps: Design and Performance", *Proceedings of IEEE National Radar Conference*, 1984.

[14] Lops M., Orsini M., "Scan by Scan Averaging CFAR", *IEE Proceedings Radar and Signal Processing*, vol.136, no.6, 1989.

[15] H. Goldman, I. Bar-David "Analysis and application of the excision CFAR detector", *IEE Proceedings, Vol. 135, Pt. F, No. 6, December 1988, pp.564 -575*

[16] Galati G., Leonardi M., Magarò P., Cavallin A., "Advanced Extraction and Thresholding Techniques for Ground Targets in High Resolution Radar in Tactical Applications", *NATO RTO SET-059*, Budapest, 15-17 October 2003.

[17] Galati G., Magarò P., Leonardi M., Cavallin A., "Data Extraction in High Resolution Surface Movement Radar for A-SMGCS", *IRS '04,* Warsaw, 19 –21 May 2004.

[18] Ferri M., Galati G., De Fazio A., Magarò P., "Millimetre-Wave Radar Applications in Airports: Experimental Results", *EuRAD '04* Amsterdam, 11 –15 October 2004.

[19] Pitas I., "Digital image processing algorithms", *Prentice Hall International Series in Acoustic, Speech, and Signal Processing*, 1993.

[20] Foresti G. L., Frassinetti M., Galati G., Marti F., Pellegrini P., Regazzoni C. S., "Image Processing Applications to Airport Surface Movements Radar Surveillance and Tracking", *Proceedings of 20th IEEE International Conference on Industrial Electronics, Control and Instrumentation*, Bologna (Italy), 05 - 09 September 1994.

[21] Galati G., Leonardi M., Magarò P., "Bearing Angle and Shape Extraction Features in High Resolution Surface Movement Radar", *RTA NATO SET-059*, Budapest, 15-17 October 2003.

[22] Galati G., Leonardi M., Magarò P., "Analysis and Evaluation of different tracking algorithms Based on Roadmap Information ", *RTA NATO SET-059*, Budapest, 15-17 October 2003.

[23] Bar Shalom Y., Blair D,. *"Multitargets-Multisensors Tracking Applications"*, Artech House, 2000.

[24] Bar Shalom Y, Xiao-Rong Li, "Estimation and Tracking: Principles, Techniques and Software" *Artech House, 1993*

[25] Bar Shalom Y, Xiao-Rong Li, "Multitarget- Multisensor Tracking: Priciples and Techniques", *YBS*, 1995

[26] Brookner, "Tracking and Kalman Filtering Made Easy" *John Wiley & Sons* 1998

[27] Blackman, Popoli, "Design and Analysis of Modern Tracking Systems", *Artech House* 1999

[28] T. Kirubarajan, Y. Bar-Shalom and K.R. Pattipati, "Topography-Based VS-IMM Estimator for Large-Scale Ground Target Tracking", *Proc. IEE Colloq. on Target Tracking, pp. 11/1--11/4, London, England, Nov. 1999*

[29] T. Kirubarajan, Y. Bar-Shalom, K. R. Pattipati, and I. Kadar, "Ground target tracking with variable structure IMM estimator," *IEEE Transactions on Aerospace and Electronic Systems, vol. 36, no. 1, pp. 26-46, 2000*.

[30] Jesús García Herrero, Juan A. Besada Portas, José R. Casar Corredera "Use of Map Information for Tracking Targets on Airport Surface", *IEEE Transactions on Aerospace and Electronic Systems, Volume 39, Nº 2, April 2003. pg 675-694*

[31] Jesús García Herrero, Juan A. Besada Portas, Francisco J. Jiménez Rodríguez, José R. Casar Corredera "Surface Movement Radar Data Processing Methods for Airport Surveillance", *IEEE Transactions on Aerospace and Electronic Systems, Volume 37, Nº 2, April 2001. pg 563-586*